Electronic Structure of the C_{60} Fragment in Alkali- and Alkaline-earth-doped Fullerides

Michael C. Böhm[a,b], Thomas Schedel-Niedrig[a], Hartmut Werner[a], Robert Schlögl[a], Joachim Schulte[b] and Johannes Schütt[b]

[a] Fritz-Haber-Institut der Max-Planck-Gesellschaft, Faradayweg 4 - 6, D-14195 Berlin
[b] Institut für Physikalische Chemie, Physikalische Chemie III, Technische Hochschule Darmstadt, Petersenstr. 20, D-64287 Darmstadt

Z. Naturforsch. **51 a,** 283–298 (1996); received February 27, 1996

The electronic structure of the C_{60} fragment in alkali- and alkaline-earth-doped fullerides is studied theoretically. With increasing metal-to-C_{60} charge transfer (CT) the π electronic properties of the soccerball are changed. In the undoped solid and for not too high a concentration of doping atoms the hexagon-hexagon (6-6) bonds show sizeable double bond character while the hexagon-pentagon (6-5) bonds are essentially of single bond type. In systems with a high concentration of doping atoms this relative ordering is changed. Now the 6-5 bonds have partial double bond character and the 6-6 bonds are essentially single bonds. The high ability of the C_{60} unit to accomodate excess electrons prevents any sizeable weakening of the overall π bonding in systems with up to 12 excess electrons on the soccerball. A crystal orbital (CO) formalism on the basis of an INDO (intermediate neglect of differential overlap) Hamiltonian has been employed to derive solid state results for potassium- and barium-doped C_{60} fullerides. For both types of doping atoms an incomplete metal-to-C_{60} CT is predicted. In the potassium-doped fullerides the magnitude of the CT depends on the interstitial site of the dopant. The solid state data have been supplemented by INDO and *ab initio* calculations on molecular C_{60}, C_{60}^{6-} and C_{60}^{12-}. The calculated bondlength alternation in the neutral molecule is changed in C_{60}^{12-} where the length of the 6-6 bonds exceeds the length of the 6-5 bonds. The geometries of the three molecular species have been optimized with a 3-21 G* basis. The theoretically derived modification of the C_{60} (π) electronic structure as a function of the electron count is explained microscopically in the framework of two quantum statistics accessible for π electronic ensembles. In the π ensemble of the C_{60} fragment so-called hard core bosonic properties are maximized where the Pauli antisymmetry principle has the character of a hidden variable only. Here the electronic degrees of freedom are attenuated only by the Pauli exclusion principle. This behaviour leads to the changes in the π electronic structure mentioned above.

1. Introduction

Alkali- and alkaline-earth-doped fullerides have been studied by many research groups because of their interesting material properties, which are documented in comprehensive review articles [1 - 4]. The C_{60} molecule is an important building-element in fullerides with non-conventional properties such as superconductivity. Experimental studies verified sizeable non-isoelectronic effects with respect to the structural or superconducting behaviour [5, 6]. Fullerides can occur as Mott-like insulators with resistivity maxima, as band insulators or semiconductors with a gap between filled and empty dispersion curves as well as conductors. A high-temperature metallic configuration is the prerequisite to render possible low-temperature superconductivity, which has been observed in alkali-doped fullerides of stoichiometry M_3C_{60} (M = K, Rb, Cs) [7, 8] as well as in the alkaline-earth-doped materials Ca_5C_{60} [9] and Ba_6C_{60} [10]. The exact stoichiometry of the Ba-doped superconductor seems to be afflicted with some uncertainties [11, 12]. On the basis of the fascinating experimental incentives, the solid state electronic structure of fullerides has been studied by many theoreticians [13, 14]. Most of the band structure investigations on alkali- and alkaline-earth-doped fullerides are based on variants of the density functional (DF) method. Typical quantities that have been evaluated

Reprint requests to Prof. Dr. M. C. Böhm, Darmstadt.

0932-0784 / 96 / 0400-0283 $ 06.00

in band structure calculations are dispersion curves, electronic density of states (DOS) distributions or Fermi surface (FS) properties. Apart from these solid state activities there exists a second research field of electronic structure investigations of fullerenes, i. e. the quantum chemical calculations of the corresponding molecular systems [15]. The expectation values considered in these studies, however, differ from those evaluated in solid state investigations. Although most of the quantum chemical calculations on fullerene molecules have been performed on neutral networks, ionic states have been considered as well [16 - 18]. An interesting analysis of highly charged fullerene molecules has been given in [19], where it has been pointed out that the π electronic structure of the corresponding systems is changed strongly in the presence of a larger number of excess electrons. But it seems that such an analysis of the fullerene fragment in alkali- and alkaline-earth-doped fulleride solids with a broad width in the net metal-to-C_{60} charge transfer (CT) is still missing.

It is the purpose of the present contribution to analyze the modification in the M_xC_{60} electronic structure of C_{60} fullerides with M abbreviating an alkali- or alkaline-earth atom. The theoretical tool of our investigation is a crystal orbital (CO) formalism derived in the framework of an INDO (intermediate neglect of differential overlap) Hamiltonian [20]. In recent contributions we have adopted this solid state approach to investigate the electronic band structure of alkali- and alkaline-earth-doped C_{60} fullerides [12, 21 - 25]. The CO method adopted renders possible the evaluation of typical band structure quantities such as DOS profiles, bandwidths or FS properties with good accuracy. In the present work we concentrate on the modification of the C_{60} (π) electronic structure as a function of the M-to-C_{60} CT. Consequently no $\boldsymbol{k}$-space properties, with $\boldsymbol{k}$ abbreviating the conventional wave vector in the band theory of solids, will be considered in this work. Although the CO Hamiltonian employed is of semiempirical nature, the computational effort of some calculations approaches the boundaries of the present days computational facilities. In this context we refer to the phase Ba_3C_{60} we have considered which crystallizes with two formula units ($z = 2$) in a primitive cubic lattice [24]. This crystal structure, e. g., leads to a CO eigenvalue problem with 126 atoms (= 504 atomic orbitals (AOs)) in the unit cell. In detail we have investigated the following potassium and barium C_{60} fullerides: K_xC_{60} (x = 1, 2, 3, 4, 6) and Ba_xC_{60} (x = 3, 4, 5, 6). In the alkali-doped series the phase diagram has been studied in detail for different donor atoms. The stoichiometry of the different phases is well known. In the phase diagram of the barium series, Ba_3C_{60} and Ba_6C_{60} have been identified unambiguously [26]. An X-ray-diffraction study has shown the presence of at least one additional phase between the above phases. In this work we have considered both Ba_4C_{60} and Ba_5C_{60} as model systems in the CO calculations. To quantify the modification in the C_{60} electronic structure as a function of the metal-to-C_{60} CT we have calculated the atomic net charges q_i in the framework of a Mulliken population analysis [27]. Although the q_i numbers confined to electropositive centers with diffuse AOs are not free of some conceptual problems [11, 28] we are convinced that the discussion of the C_{60} data and the consequences drawn from these results are not ambiguous. A recent DF study of Ba_6C_{60} has shown that the Ba net charge either derived by a Mulliken population analysis or a volume integration only differs quantitatively but leads to the same general trend [11]. In alkaline-earth-doped fullerides many experimental and theoretical contributions agree in so far that they predict a strong hybridization which implies an incomplete transfer of the alkaline-earth valence electrons to the C_{60} soccerball [11, 29 - 32]. In alkali-doped fullerides the magnitude of the CT is still a subject of some controversial discussions. Certain band structure approaches, most of which are based on DF variants, predict an almost complete valence ionization [13, 14, 33]. There are however experimental observations supporting an incomplete CT. These are Raman spectra [34], hindered C_{60} rotations in doped materials [35], the modification of the lattice constants in the series M_xC_{60} [36] as well as photoemission data [37]. In [21] we have shown that the photoemission spectrum of K_3C_{60} can be reproduced trustworthily only by a theoretical model which leads to different alkali net charges at the two crystallographically non-equivalent doping centers; see below. The doped fullerides which have been selected as model systems cover a large width as far as the charge excess on the soccerball is concerned. The accompanying modification in the fullerene electronic structure will be discussed on the basis of atomic net charges q_i and so-called Wiberg bond indices $W_{CC'}$, which are a measure of the covalent interaction between bonded atomic centers [38]. On the basis of the $W_{CC'}$ elements one can discriminate between, e. g., double and single bonds. The theoretical discussion

Table 1. Space groups (SG), Bravais lattices (BL), unit cell dimensions *a*, *b*, *c* (in pm) and K, Ba fractional coordinates in C_{60}, K_xC_{60} and Ba_xC_{60} fullerides. Ba_3C_{60} has been calculated with $z = 2$ stoichiometric units per unit cell; all other systems have been defined with $z = 1$. The labels t and o in some of the potassium fullerides symbolize tetrahedral and octahedral occupancies in the fcc lattice. For Ba_5C_{60} two structural suggestions have been considered.

System	SG	BL	*a*	*b*	*c*	*x*	*y*	*z*
C_{60}	$Fm\bar{3}$	fcc	1419.8					
K_1C_{60}	$Fm\bar{3}$	fcc	1419.8			0.50	0.50	0.50 (o)
K_2C_{60}	$Fm\bar{3}$	fcc	1419.8			0.25	0.25	0.25 (t)
						0.75	0.75	0.75 (t)
K_3C_{60}	$Fm\bar{3}$	fcc	1419.8			0.50	0.50	0.50 (o)
						0.25	0.25	0.25 (t)
						0.75	0.75	0.75 (t)
K_4C_{60}	Immm	bco	1186.6	1077.4		0.28	0.50	0.00
						−0.28	0.50	0.00
						0.50	0.28	0.00
						0.50	−0.28	0.00
K_6C_{60}	$Im\bar{3}$	bcc	1138.5			0.28	0.00	0.50
						−0.28	0.00	0.50
						0.50	0.28	0.00
						0.50	−0.28	0.00
						0.00	0.50	0.28
						0.00	0.50	−0.28
Ba_3C_{60}	$Pm\bar{3}n$	pc	1134.3			0.25	0.00	0.50
						0.50	0.25	0.00
						0.00	0.50	0.25
						0.75	0.00	0.50
						0.50	0.75	0.00
						0.00	0.50	0.75
Ba_4C_{60}	Immm	bco	1125.0	1160.0	1090.0	0.22	0.50	0.00
						0.50	0.28	0.00
						0.50	−0.28	0.00
						−0.22	0.50	0.00
$Ba_5C_{60}(1)$	$Fm\bar{3}$	fcc	1419.8			0.25	0.25	0.25
						0.40	0.40	0.40
						−0.40	−0.40	0.40
						−0.40	0.40	−0.40
						0.40	−0.40	−0.40
$Ba_5C_{60}(2)$	Immm	bco	1117.1	1117.1	1117.1	0.50	0.28	0.00
						0.50	−0.28	0.00
						0.28	0.00	0.50
						−0.28	0.00	0.50
						0.00	0.50	0.28
Ba_6C_{60}	$Im\bar{3}$	bcc	1117.1			0.50	0.28	0.00
						0.50	−0.28	0.00
						0.28	0.00	0.50
						−0.28	0.00	0.50
						0.00	0.50	0.28
						0.00	0.50	−0.28

of the solid state properties of doped fullerides on the basis of the INDO CO data will be supplemented by INDO MO [39] and *ab initio* [40] calculations of the C_{60} molecule and two of its highly charged ions. We have used the GAMESS program to derive the optimized geometries of C_{60}, C_{60}^{6-} and C_{60}^{12-}. The basis set employed is of 3-21 G* quality. The molecular variant of the present INDO formalism [39] has been adopted to analyze the π orbitals of C_{60} as well as the above mentioned ions in a basis of localized molecular orbitals (LMOs). The first and greater part of this article concerns the modification of the C_{60} electronic structure as a function of the electron count as it results from quantum chemical calculations. The second major objective of the article is tackled in the last chapter, where we give a microscopic explanation of these computational findings. This explanation is based on quantum statistical considerations and therefore on quite general distinctions between different π electronic ensembles.

The outline of the present contribution is as follows. The crystallographic data of the fullerides studied are described in the next section. The computational conditions used in the semiempirical CO and MO as well as *ab initio* calculations are mentioned Section 3. The theoretical results are then discussed in Section 4. The article ends with a resume where we explain the microscopic origin of the modification of the C_{60} electronic structure as a function of the CT. The computational facilities employed, as well as the space and CPU time demands are mentioned in an appendix.

2. Geometries

In all CO calculations we have employed a C_{60} unit with perfect icosahedral I_h symmetry. In the soccerball the C atoms form 20 hexagons and 12 pentagons, an arrangement which leads to two sets of CC bonds. 30 bonds are shared between neighbouring hexagons and 60 bonds are formed by hexagon-pentagon contacts. The first set will be abbreviated by the label 6-6 and the latter one by 6-5. In the CO calculations of the fullerides we have adopted a common length of the two sets of CC bonds. We have used the experimental values of the undoped C_{60} system, i. e. 139.6 pm for the 6-6 and 143.9 pm for the 6-5 bonds [41]. This choice allows us to analyze changes in the C_{60} electronic structure which are caused by the number of electrons per soccerball or intermolecular (= solid state) spatial degrees of freedom, and not by any intramolecular geometric changes. We wish to point out that the quantities we have studied (i. e. atomic net charges, Wiberg bond indices) depend only weakly on the intramolecular CC bondlengths.

The structural data used as input in the solid state calculations of doped fullerides have been summarized in Table 1. We have given the space group (SG),

the Bravais lattice (BL), the unit cell dimension as well as the atomic positions of the dopant atoms in terms of fractional coordinates. Most of the unit cell parameters in the table are based on X-ray investigations [10, 26, 42 - 44]. For phases which can not yet be investigated crystallographically we have extrapolated the structural data from related systems. This proceeding, e.g., has been necessary in the case of Ba_5C_{60}; see below. Undoped C_{60} and alkali-doped fullerides K_xC_{60} with $x = 1, 2, 3$ crystallize in a fcc lattice with two tetrahedral (t) and one octahedral (o) interstitial sites. In K_3C_{60} all interstitial sites are occupied by potassium atoms. Tetrahedral site occupancy has been assumed in K_2C_{60}, a pattern realized in Na_2C_{60}. For K_1C_{60}, o occupancy has been employed in the CO approach, a solid state geometry detected in M_1C_{60} with M = Rb and Cs. Experimental work has lead to the suggestion that a temperature dependent occupancy of t and o sites is realized in the corresponding potassium system. Doping beyond $x = 3$ requires a structural modification because all interstitial sites of the fcc lattice are occupied for $x = 3$. For K_4C_{60} we have assumed a body-centered orthorhombic (bco) lattice with space group symmetry Immm. The positions of the K atoms correspond to distorted tetrahedra. The orthorhombic structure is forced by ordered C_{60} units leading to two types of crystallographically non-equivalent positions of the dopant atoms. A body-centered cubic (bcc) structure has been adopted for K_6C_{60}. By analogy with K_4C_{60}, the K atoms fill distorted tetrahedra. Note that the size of the octahedral cage exceeds the size of the tetrahedral one by far [23].

As shown in Table 1 the crystal structures of the alkali- and alkaline-earth-doped fullerides coincide in the systems with $x = 4$ and 6. As mentioned above a primitive cubic lattice with $z = 2$ is established in Ba_3C_{60} [24]. The space group we have used is $Pm\bar{3}n$. In this space group the soccerball centers are ordered on a bcc sublattice. The Ba atoms face pentagons only. Finally we have to comment on the crystal structure(s) employed for Ba_5C_{60}. An unambiguous identification of this phase via X-ray diffraction has not been feasible yet. Therefore we have adopted two plausible structural suggestions. Structure 1 (= $Ba_5C_{60}(1)$) has been transferred from Ca_5C_{60} which forms a fcc lattice [45]. Here four Ca atoms are located at the o site where they form some type of Ca_4 tetrahedron. The fifth Ca atom occupies one of the two t interstitial sites of the fcc lattice, the second one remains

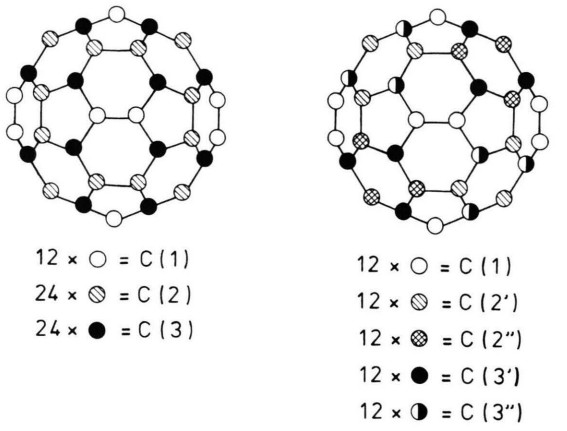

Fig. 1. Non-equivalent carbon positions in fcc, bcc ($\neq Ba_5C_{60}$) and pc fullerides (representation on the lhs.) and fcc Ba_5C_{60} (= $Ba_5C_{60}(1)$, rhs.) On the lhs. we have used the labels C(1), C(2), C(3) to discriminate between non-equivalent C atoms. The atomic labels adopted for Ba_5C_{60} indicate their origin in the diagram on the lhs.

empty. The second Ba_5C_{60} structure (= $Ba_5C_{60}(2)$) we have considered has been extrapolated from the Ba_6C_{60} structure where one distorted tetrahedral site of the bcc lattice remains unoccupied [10]. In the CO calculation $a = b = c$ (a, b, c = lattice constants) has been assumed.

Adoption of the structures summarized in Table 1 and ordering of the soccerballs leads to three non-equivalent C positions in the bcc lattice of the $x = 6$ fullerides. This threefold splitting of the C atoms is also realized in C_{60} and K_xC_{60} ($x = 1, 2, 3$), which crystallize in a fcc lattice, as well as in Ba_3C_{60}, which is primitive cubic. In the fcc structure of Ba_5C_{60}, i. e. $Ba_5C_{60}(1)$, five crystallographically non-equivalent carbon sites occur. A schematic representation showing the splitting of the C atoms of C_{60} into three and five non-equivalent positions is given in Figure 1. In the diagram the multiplicity of the corresponding positions is indicated. In the bco lattice of K_4C_{60} and Ba_4C_{60} nine non-equivalent C positions are realized. Six of them have a multiplicity of eight, the remaining three a multiplicity of four. The splitting pattern of the C atoms in the second Ba_5C_{60} model is of larger complexity. It is not discussed in detail in the present work. For more details concerning the mutual spatial orientation between the different C positions and the interstitial sites in doped fullerides we refer to [23].

We have already mentioned that two sets of CC bonds occur in the icosahedral C_{60} molecule, i. e. the 6-6 and 6-5 bonds. In the solid state this number is

enlarged as a result of the non-equivalent carbon positions. In the bcc lattice five different CC bonds are found. The same number is realized in the other fullerides with three crystallographically non-equivalent carbon sites. In both lattices we find two different 6-6 bonds and three 6-5 bonds. In $Ba_5C_{60}(1)$ eight different CC bonds decompose into three 6-6 and five 6-5 pairs. In the bco systems K_4C_{60} and Ba_4C_{60}, 15 different CC bonds are are formed. Six are of the 6-6 type, the remaining nine are 6-5 bonds.

3. Computational Conditions

The theoretical basis of the INDO CO approach has been discussed in [20], while the molecular precursor has been defined in [39]. Previous applications of the CO method to doped fullerides have been given in [12, 21 - 25]. The theoretical steps to simulate Ba atoms in the present CO formalism are described in [24]. The capability but also the limitations of the band structure formalism have been described in a review [46]. The computational conditions employed in the CO calculations coincide with those adopted in our recent investigations of fullerides. In the present work we have studied two types of one-determinantal solutions of the CO Hamiltonian, i. e. insulating or semiconducting states with an energetic separation between filled and empty dispersion curves and metallic states with a partially filled conduction band. In some of our recent contributions on doped fullerides [22, 23, 25] we have discussed explicitly the strong competition between metallic configurations on the one hand and insulating Mott-states on the other, where the number of singly occupied one-electron states in the highest filled band(s) corresponds to a maximum. Mott-states are established in solids with a narrow conduction band in the presence of strong two-electron repulsions. For the quantities we have considered in this work it is however irrelevant whether the ground state is metallic or Mott-like. The magnitude of the metal-to-C_{60} CT and the real-space quantities confined to the soccerball are roughly the same in both electronic configurations. Therefore we have neglected this additional electronic degree of freedom in the subsequent discussion.

Application of the CO approach requires the subdivision of the overall crystal volume into two types of spatial domains A and B. Domain A has to be defined for each atomic site. Within the corresponding atomic spheres the self-consistent-field (SCF) equations in the CO basis are solved exactly in the given degree of sophistication. The interatomic interaction outside these atomic spheres, i. e. in domain B, is approximated by the classical Madelung potential. On the basis of test calculations we have selected a common atomic radius of 700 pm [47]. For the numerical integrations in $\boldsymbol{k}$-space we have adopted a generalization of the so-called large unit cell (LUC) method [48], which makes use of the Patterson symmetry in reciprocal space [49]. The integration domains generated by this setup frequently are of simpler geometric structure than those of conventional Brillouin zones (BZ). With one exception (i. e. Ba_3C_{60}) the Patterson symmetry of the solids studied coincides with the SG symmetry; see Table 1. The Patterson symmetry associated to the Ba_3C_{60} space group symmetry $Pm\bar{3}n$ is $Pm\bar{3}m$.

Table 2. Number of $\boldsymbol{k}$-points considered in the irreducible part of the Brillouin zone (IBZ) and the total Brillouin zone (BZ) in the CO calculations of the M_xC_{60} fullerides.

System	$\boldsymbol{k}$-grid IBZ	$\boldsymbol{k}$-grid BZ
C_{60}	22	264
K_1C_{60}	22	264
K_2C_{60}	22	264
K_3C_{60}	22	264
K_4C_{60}	54	216
K_6C_{60}	14	168
Ba_3C_{60}	10	240
Ba_4C_{60}	54	216
$Ba_5C_{60}(1)$	22	264
$Ba_5C_{60}(2)$	56	216
Ba_6C_{60}	14	168

In Table 2 we have collected the number of $\boldsymbol{k}$-points considered in the irreducible part of the Brillouin zone (IBZ) together with the number of $\boldsymbol{k}$-points in the total BZ. The dimension of the grids adopted in this work exceeds the number of $\boldsymbol{k}$-points of many band structure investigations of fullerides [13, 14, 33]. Table 2 may indicate the high expenditure of computer facility which had been necessary in the present investigation. A Hartree damping of the bond-order matrices has been adopted to suppress convergence problems during the SCF iterations.

To elucidate electronic consequences which are manifested in the Wiberg bond indices $W_{CC'}$ derived for the solid state systems we have studied the electronic structure of molecular C_{60}, C_{60}^{6-} and C_{60}^{12-} in a basis of LMOs. We have used the Edmiston-Ruedenberg localization procedure to transform the

canonical MOs into LMOs [50]. The C_{60} geometries adopted in this step coincide with the solid state geometries. Finally we have used the GAMESS program to optimize the geometry of these three molecules [40]. This proceeding has been useful to quantify the response of the carbon nuclei on the modification of the C_{60} electronic structure with increasing charge excess. As mentioned above, the basis set employed is of 3-21 G* quality, a computational setup leading to 540 basis functions. Of course it is impossible to optimize all 174 (i.e. 3*60 – 6) atomic degrees of freedom of these molecules independently. Therefore we have started the geometry optimization from subgroups of the icosahedral I_h group. We have used the point symmetries D_{5d}, D_{3d} and D_{2h} which correspond to Jahn-Teller-distorted C_{60} geometries. The selection of different starting configurations should render possible the detection of the global minimum and not a local one. The *ab initio* calculations lead to identical optimized space group symmetries of the three molecular systems considered, independent of the starting configuration.

4. Results and Discussion

We start the discussion of the CO results with the atomic net charges at the dopant and carbon centers q_d and q_i in both series of fullerides. The q_d numbers are displayed in Fig. 2, the carbon net charges in Figs. 3 and 4. For reasons of completeness we have added the atomic net charges of the undoped C_{60} solid to the two latter diagrams. Figure 2 indicates that K and Ba differ in their oxidation state. The K net charges are always smaller than +1.0. They show a clear distinction between potassium t and o centers. In all Ba-doped fullerenes the Ba net charges are slightly larger than +1.0 . Both types of dopant atoms, however, deviate strongly from the limit of complete valence ionization. Metal-C_{60} hybridization occurs in both families of doped fullerides. We already have emphasized that the CO results derived for the Ba fullerides agree with previous experimental and theoretical findings [11, 29 - 32]. For the K-doped fullerides we refer to the discussions given in [21, 34 - 37]. In the Ba_xC_{60} series we find an increasing Ba-to-C_{60} CT with increasing doping. The electronic origin leading to different Ba net charges in the two Ba_5C_{60} models has been discussed in a separate article [25]. In the K-series the charge deficit at the o site exceeds the one at the t sites. Obviously a larger size of the interstitial cage

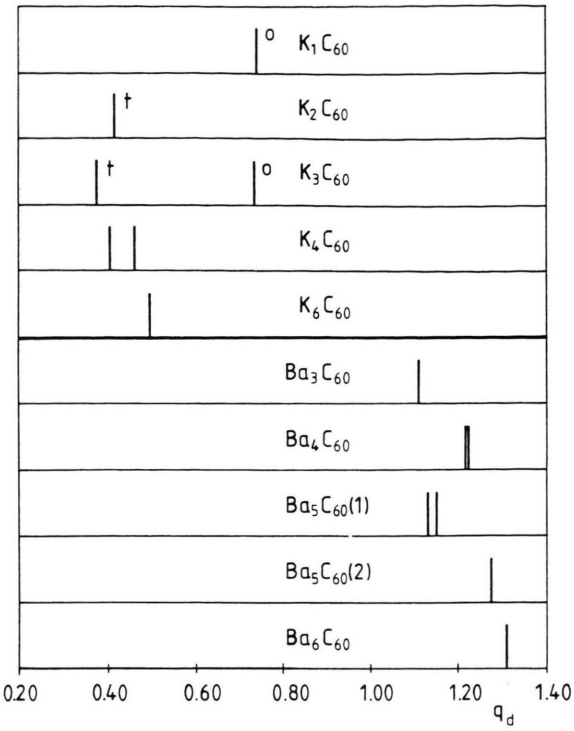

Fig. 2. Net charges at the doping atoms potassium and barium q_d calculated for both series of C_{60} fullerides. The labels t and o indicate tetrahedral and octahedral occupancies in the fcc lattice of the potassium fullerides.

causes a stronger alkali ionization, a computational result that can be explained as follows. The overlap between the potassium and carbon wave functions is rather small for the o occupancy. Bonding then is accessible only via the long-range Coulomb attraction. Covalent bonding contributions, however, can compete successfully with the electrostatic interaction in the coupling between the potassium t site and C_{60}. The covalent interaction in the barium fullerides profits quite generally from the somewhat smaller unit cell dimensions of the Ba_xC_{60} systems in comparison to the lattice spacings of the K_xC_{60} materials. Note that the covalent and ionic radii of K and Ba are roughly the same. Before discussing the charge distribution in the C_{60} unit we want to mention that minimal basis-set Hamiltonians of the zero differential overlap (ZDO) type tend to overestimate the covalency of alkali- and alkaline-earth-carbon bonds [28]. Therefore it cannot be ruled out that the calculated metal-to-C_{60} CT corresponds to a lower boundary. But as shown below, such a possible deviation from the "exact" CT will not lead to any principal problems in our argumentation.

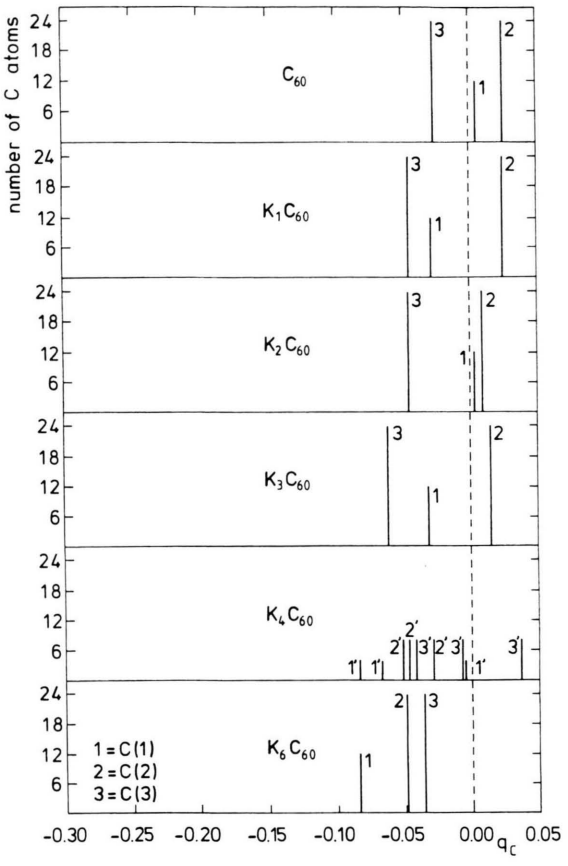

Fig. 3. Carbon net charges q_i calculated for crystalline C_{60} (top diagram) and K_xC_{60} fullerides. The numbers in the diagram refer to the non-equivalent C atoms shown in Figure 1. The bco lattice of K_4C_{60} leads to nine different C sites. The labels 1', etc. symbolize the origin of the corresponding atoms in the fcc and bcc lattice. The height of each peak measures the multiplicity of the atom under question.

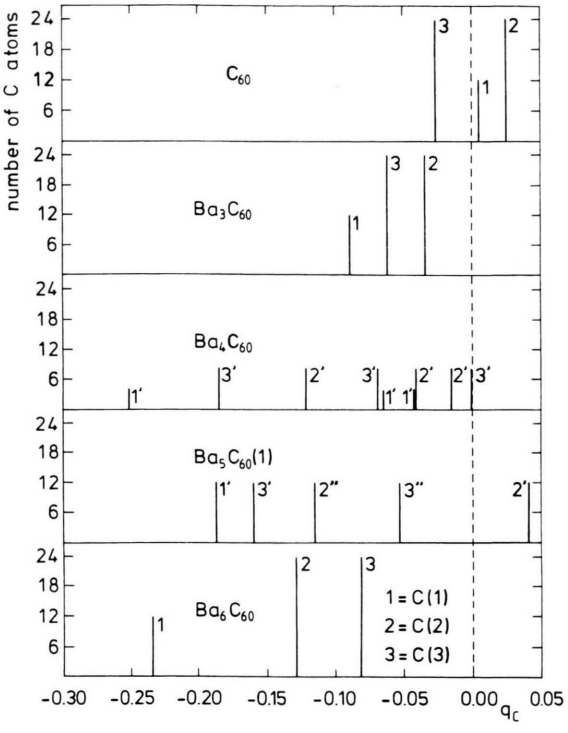

Fig. 4. Carbon net charges q_i calculated for crystalline C_{60} (top diagram) and Ba_xC_{60} fullerides except $Ba_5C_{60}(2)$; see legend Figure 3. The atomic numbering scheme used in Ba_5C_{60} has been defined in Figure 1.

The different carbon net charges in Figs. 3 and 4 are a consequence of the soccerball ordering, a process which is responsible for the crystallographically non-equivalent C centers discussed in Section 2. The q_i numbers derived for the undoped C_{60} solid visualize the high symmetry constraints in the isolated C_{60} molecule. To our best knowledge, C_{60} is the only polycyclic nonalternant carbon framework where the high molecular symmetry prevents a non-even charge distribution which usually is considered as a key-quantity of these molecules. Removal of the icosahedral symmetry constraint in the solid renders possible a polarization of the (π) electron distribution of C_{60}. Figure 3 shows that this charge reorganization is not enhanced furthermore by the K atoms. In the K_xC_{60} series with $x \leq 4$, carbon centers with a charge deficit survive in the neighborhood of centers with a charge excess. With exception of $Ba_5C_{60}(1)$, q_i elements > 0 do not occur in the Ba_xC_{60} fullerides. Here they are more or less prevented by the stronger metal-to-C_{60} CT. Comparison of Figs. 3 and 4 visualizes that the overall width in the q_i distribution is of the same order of magnitude in K_3C_{60} and Ba_3C_{60}, but differs sizeably for the pair K_4C_{60} and Ba_4C_{60}. The $x = 6$ fullerides are between these two pairs.

Next we analyze the Wiberg bond indices $W_{CC'}$ of both fulleride series; see Figures 5 and 6. For reasons of completeness we have added the $W_{CC'}$ numbers of the undoped C_{60} solid to both representations (top diagram). To enhance the comprehensibility of the comparative discussion we have given the net charge on the soccerball q_f of each doped system which has been considered in the two figures. The $W_{CC'}$ are defined by the sum of the squares of all bond order matrix elements between the diatomic pair in question.

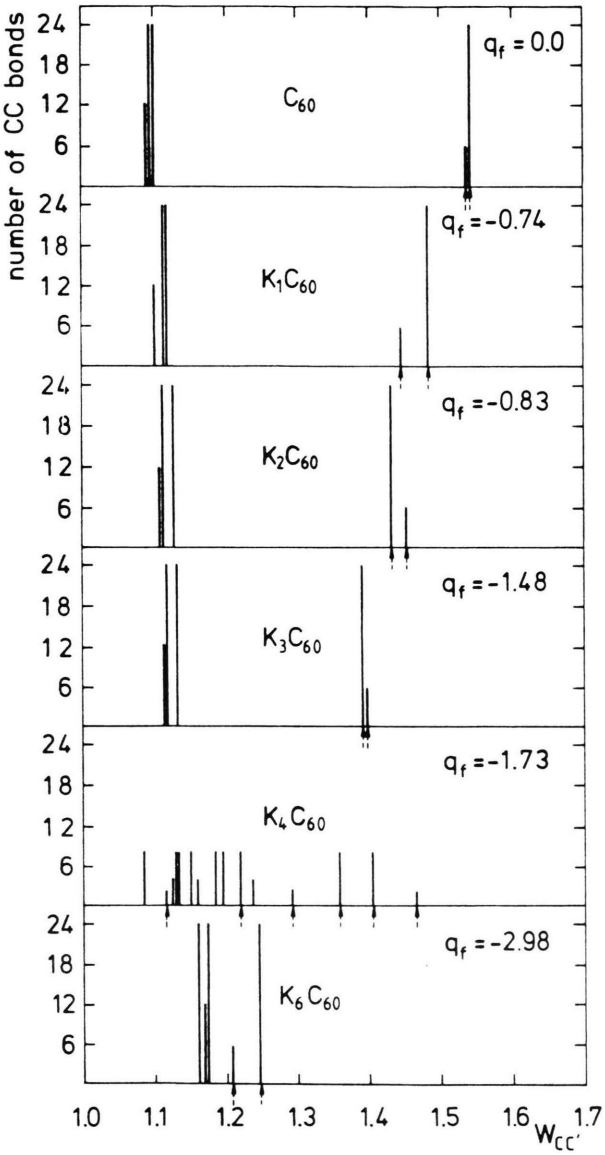

Fig. 5. Wiberg bond indices $W_{CC'}$ of the C_{60} solid and all K_xC_{60} fullerides considered. The multiplicity of the corresponding indices is indicated on the ordinate. The 6-6 bonds are labeled by a broken arrow. q_f represents the net charge on the C_{60} soccerball.

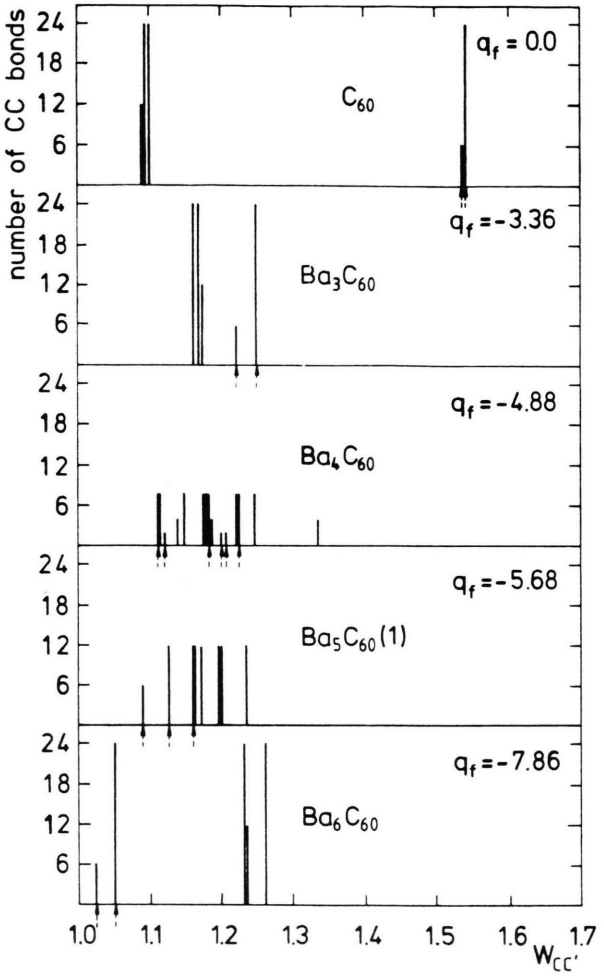

Fig. 6. Wiberg bond indices of the C_{60} solid and Ba_xC_{60} fullerides except Ba_5C_{60}(2); see legend of Figure 5.

In CO methods, the corresponding bond orders have to be integrated over all values of the $\boldsymbol{k}$-vector. The sum of the squared bond order matrix elements corresponds to the number of covalent bonds formed by the atom pair under consideration (corrected for the ionic character of the bond). This means that the $W_{CC'}$ of a homopolar single bond amounts to 1.0 while the value of an isolated double bond is 2.0. We wish to point out that the σ-type interaction in all molecular C_{60} systems and the doped fullerides leads to a $W_{CC'}$ of 1.0. $W_{CC'}$ elements > 1.0 are caused by π-type interactions. In the following we will deal with this effect. In the undoped solid one finds that the $W_{CC'}$ parameters of the 6-6 bonds exceed the Wiberg bond indices of the 6-5 bonds by far. The 6-5 indices are essentially of single bond type with small double bond admixtures. The K-to-C_{60} CT leads to a population of the t_{1u} π^* LUMO (lowest unoccupied molecular orbital) of the undoped C_{60} system. This "molecular label" should be accepted as a formal classification only. The metal-C_{60} hybridization in the doped solids causes a strong intermixing of unperturbed C_{60}

orbitals and AOs of the alkali donors. Furthermore it should be mentioned that also the label "π^* orbital" corresponds to a simplified description. The icosahedral geometry of C_{60} leads to an allowed π/σ and π^*/σ^* coupling in the SCF wave function, a mechanism which is absent in planar π systems. In [23] we have given a quantitative analysis of this interaction. π and π^* admixtures are the leading elements in the highest filled and lowest empty C_{60} orbitals. In the inner valence region we have observed strong intermixing of these "in-plane" (= σ) and "out-of-plane" (= π) orbitals. The LMOs discussed below, however, are of bare π or π^* type with negligible admixtures from in-plane AOs. With increasing population of the t_{1u} LUMO the double bond character of the 6-6 bonds is continuously reduced while it is enhanced for the 6-5 bonds. To estimate the observed changes of the $W_{CC'}$ numbers critically it has to be taken into account that 30 6-6 bonds compete with 60 6-5 bonds. The clear graduation between both types of bond indices is lifted in orthorhombic K_4C_{60}, where both sets of $W_{CC'}$ elements are intermixed. This is caused by the low crystal symmetry of this system. Remember that a common soccerball geometry has been employed in all CO calculations. The sequence of the Wiberg indices as realized in the undoped solid and potassium fullerides with $x \leq 3$ is restored in K_6C_{60}. The difference between both sets of $W_{CC'}$ elements, however, is much smaller than in systems with $x \leq 3$.

The ordering of the two sets of $W_{CC'}$ parameters is changed in the barium fullerides with higher doping concentrations. The larger number of valence electrons in this series leads to the population of hybridized C_{60} (LUMO+1) π^* states of t_{1g} symmetry for $x > 3$. Figures 5 and 6 show that the bond indices of Ba_3C_{60} and K_6C_{60} are roughly the same. In consideration of the similiar C_{60} excess charge this result could be expected. By analogy with K_4C_{60} the sequence of the bond indices associated to the 6-6 and 6-5 bonds is intermixed in Ba_4C_{60} which - just as K_4C_{60} - crystallizes in a bco lattice. In the Ba_5C_{60} system considered in Fig. 6 and Ba_6C_{60} the calculated Wiberg indices of the 6-5 bonds exceed the 6-6 values. The 6-6 bonds in Ba_6C_{60} are almost pure single bonds while the 6-5 bonds show partial double bond character. The CO results of Figs. 5 and 6 can be interpreted as follows. With increasing excess charge on the C_{60} soccerball (= increasing population of hybridized LUMO and (LUMO+1) states of t_{1u} and t_{1g} symmetry) the character of the two sets of CC bonds

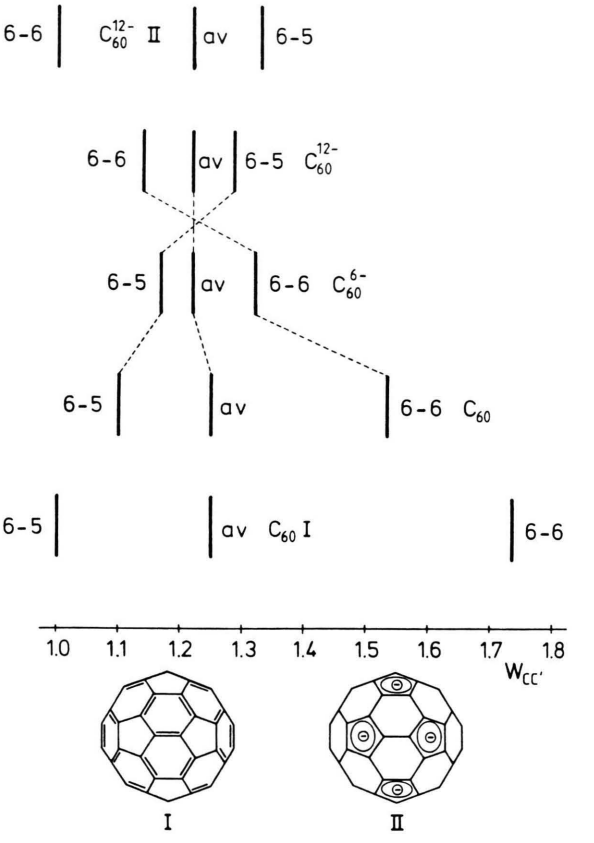

Fig. 7. Wiberg bond indices $W_{CC'}$ of the C_{60} molecule, C_{60}^{6-} and C_{60}^{12-} according to INDO MO calculations (central part of the diagram). The label av symbolizes the mean value of the bond index (= W_{av}) averaged over the 90 bonds of the C_{60} unit. In the bottom and head line of the $W_{CC'}$ diagram we have given the bond indices associated to the C_{60} electronic structure I with localized (= electronically isolated) 6-6 double bonds and to the C_{60}^{12-} electronic structure II with isolated π electron sextets in the pentagon rings.

is changed. In highly doped C_{60} fullerides the "original" partial π double bond character of the 6-6 bonds (reference: undoped C_{60} parent) is suppressed completely, while it is enhanced for the 6-5 bonds. This "transformation" must lead to a reduction in the maximum $W_{CC'}$ parameters as two 6-5 bonds per C atom compete with one 6-6 bond.

The interpretation of the solid state results can be made more transparent if we consider the C_{60} molecule and the two anions mentioned above. In the center part of Fig. 7 we have displayed the Wiberg bond indices of these species. They have been derived by the molecular variant of the present INDO model [39]. We have chosen a common soccerball

geometry of all molecular systems; see description in Section 2. In the schematic display we have correlated the SCF results of C_{60}, C_{60}^{6-} and C_{60}^{12-} with the Wiberg indices which have been derived for the two "resonance structures" denoted as I and II (bottom of the diagram). In picture I the 60 π electrons of C_{60} are assigned to a set of 30 localized double bonds shared by hexagon-hexagon edges. This electronic structure does not allow any delocalization over the pentagonal edges. The proximity of the $W_{CC'}$ elements of C_{60} to the bond indices of the localized picture I is clearly seen. The second picture symbolized in the bottom part of Fig. 7, i.e. II, corresponds to an assembly of 12 pentagon islands with six π electrons in each unit. This electronic structure requires 12 excess electrons per C_{60} soccerball. In Fig. 7 it is shown that the electronic system of C_{60}^{12-} approaches this boundary structure II. In C_{60}^{6-} both marginal structures I and II contribute with large weight to the SCF wave function. For C_{60} and the two anions we have calculated the mean Wiberg bond index W_{av}, i.e. the $W_{CC'}$ parameter averaged over the 90 bonds of the soccerball. W_{av} has been given in Fig. 7 as well. It can be seen that the population of the t_{1u} LUMO and t_{1g} (LUMO+1) π^* orbitals does not lead to any sizeable reduction of W_{av}, a theoretical result which indicates that the C_{60} unit is an electron deficient molecule. With increasing population of these MOs some kind of electronic switch is activated that interconverts the bonding character of the 6-6 and 6-5 bonds under conservation of the average π bonding. Consequently, excess electrons in the t_{1u} and t_{1g} MOs do not lead to an overall weakening of the π electron bonding. The theoretical findings shown schematically in Fig. 7 are in line with many experimental observations: i) C_{60} has a high electron affinity [51]. On the one hand this is caused by the pure π electronic effect described above, on the other by π^*/σ^* coupling [23]. ii) In solution the molecule can add up to six electrons reversibly [52]. iii) In reactions with organometallic compounds, C_{60} shows the characteristics of an electron deficient molecule [53]. The ability of C_{60} to accept excess electrons is related to the presence of pentagon defects in an otherwise graphitic structure [19].

Let us now move back to the doped fulleride solids and thus to the $W_{CC'}$ numbers visualized in Figures 5 and 6. The potassium systems with $x \leq 3$ have bond indices intermediate between C_{60} and C_{60}^{6-} while K_6C_{60} reproduces the C_{60}^{6-} pattern. The Ba fullerides show a graduation in their $W_{CC'}$ elements that resembles the transition between C_{60}^{6-} and C_{60}^{12-}. Please note that Ba_6C_{60} exhibits bond indices that are close to picture II of C_{60}^{12-}, although the fullerene excess charge in the alkaline-earth-doped solid is smaller (–7.86) than the value of –12 in the corresponding anion. It is of some interest to analyze the average CC Wiberg bond index W_{av} in the two series of doped fullerides. These numbers are collected in Table 3 together with the W_{av} element of the three molecular systems studied and the undoped C_{60} solid. Additionally we have calculated a so-called "defect index" W_d which is defined in the table. This number measures the reduction in the CC coupling due to covalent alkali- or alkaline-earth-C_{60} interactions. Potassium or barium doping does not lead to a strong attenuation of the average CC index of the C_{60} fragment. Of course such a behaviour has been expected on the basis of the results collected in Figure 7. The magnitude of W_d is enhanced with increasing concentration of dopants (= increasing covalent interactions between M and the C_{60} fragment). The larger W_d values encountered in the Ba fullerides in comparison to the K systems with the same x indicate the stronger hybridization in the alkaline-earth-doped fullerides.

Table 3. Mean value of the Wiberg bond index W_{av} averaged over all 90 bonds of the C_{60} molecule, the C_{60}^{6-} and C_{60}^{12-} ions and the two fulleride series according to INDO MO and CO calculations. W_d is a so-called "defect index" which measures the reduction of the actual $W_{CC'}$ parameter relative to the bare C_{60} system as a result of covalent carbon-dopant interactions.

System	W_{av}	$W_d = 90[W_{av}(\text{system}) - W_{av}(C_{60})]$
C_{60} molecule	1.246	
C_{60}^{6-} ion	1.219	
C_{60}^{12-} ion	1.221	
C_{60} solid	1.243	
K_1C_{60}	1.234	–1.08
K_2C_{60}	1.223	–2.07
K_3C_{60}	1.213	–2.97
K_4C_{60}	1.205	–3.69
K_6C_{60}	1.191	–4.95
Ba_3C_{60}	1.194	–4.68
Ba_4C_{60}	1.184	–5.58
$Ba_5C_{60}(1)$	1.172	–6.66
Ba_6C_{60}	1.178	–6.12

Localized molecular orbitals (LMOs) are a convenient diagnostic tool to describe the modification of the C_{60} π electronic structure as a function of the electron count (= excess charge). We have adopted

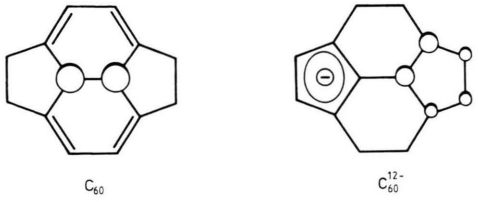

Fig. 8. Schematic representation of a localized π-type MO in the C_{60} molecule (lhs.) and C_{60}^{12-} anion (rhs.) derived by the Edmiston-Ruedenberg localization procedure. We have adopted two hexagon and pentagon units of the C_{60} molecule to visualize the LMOs. The orbitals have been symbolized schemetically in terms of the leading expansion coefficients of the π-type AOs at the "reference centers". The representation employed shows the proximity of the π-type LMOs to either the C_{60} "resonance structure" I or the C_{60}^{12-} "resonance structure" II (see bottom of Figure 7).

the three finite molecular networks considered in this study to transform the canonical MOs into a set of localized MOs. In all systems we have observed σ-type LMOs whose squared expansion coefficients (= amplitudes) at the reference centers exceed 99 %. 90 such LMOs occur. In contrast to the canonical MOs (= COs in solids), π and σ or π^* and σ^* contributions are decoupled in the LMO basis. In the C_{60} molecule, 30 π-type LMOs are evaluated with 88 % localization at two atomic sites forming a 6-6 bond. The remaining amplitudes encountered in the corresponding MO mix 6-5 as well as neighbouring 6-6 π-type contributions to the "reference function". See Fig. 8 for a simplified schematic representation of such a C_{60} π-type LMO. The localized π-type MOs evaluated for C_{60}^{12-} show a completely different behaviour. Here 94 % of the squared MO expansion coefficients are provided by the AOs of one pentagon. 36 of these "localized" π MOs are observed. Of course, the formation of localized two-center orbitals is no longer possible in C_{60}^{12-} [54]. A schematic representation of such a C_{60}^{12-} π-type LMO is also given in Figure 8. Only 6 % of the amplitudes are due to 6-6 bonds. In the C_{60}^{6-} system, LMOs as shown schematically in Fig. 8 are no longer feasible. Here the Edmiston-Ruedenberg procedure yields 30 π-type LMOs whose squared expansion coefficients confined to a certain 6-6 bond are reduced to 82 %. Note that 88 % localization has been observed in neutral C_{60}. The three remaining π-type orbitals of C_{60}^{6-} in the localized basis have non-negligible amplitudes which are scattered over all C sites of the soccerball.

Up to now we have analyzed the influence of excess charges on the π electronic structure of the C_{60} fragment in terms of Wiberg bond indices and the analytic shape of the localized π-type MOs. At the end of this section we present optimized geometries of the C_{60} molecule as well as C_{60}^{6-} and C_{60}^{12-}. The results of the *ab initio* 3-21 G* calculations can be found in Table 4. As mentioned above, we have started the optimization runs from subgroups of the icosahedral point symmetry. In all calculations the high icosahedral I_h symmetry has been restored. In C_{60}^{12-}, however, some smaller deviations from the perfect icosahedral point symmetry have been observed. The bondlength alternation of the neutral C_{60} system is overestimated by the *ab initio* approach by a factor of two. In previous quantum chemical publications it has been shown that better agreement between theory and experiment is accessible by calculations beyond the mean field approximation, e. g. a Moeller-Plesset approach in second order of perturbation [15]. The calculated bondlength alternation in neutral C_{60} of roughly 8.6 pm with the 6-5 bonds longer than the 6-6 bonds is reduced to about 2.3 pm in C_{60}^{6-}. It is switched in C_{60}^{12-}, where the length of the 6-6 bonds exceeds the 6-5 length by more than 6 pm. The rather detailed discussion of the Wiberg bond indices, which are model parameters and not an expectation value, thus can be justified in retrospect. Note the strong correlation between bondlength alternation and $W_{CC'}$ enhancement. In the context of the above computational results we refer to other *ab initio* Hartree Fock and density functional calculations which have shown similiar trends in the variation of the CC bondlengths as a function of the fullerene excess charge [17, 18]. According to a Car-Parrinello approach, $Li_{12}C_{60}$ should be a stable molecular species [18]. In the present work we have demonstrated that the switching of the C_{60} π electronic structure with increasing excess charge has a strong influence on the bondlength alternation of the soccerball. The carbon nuclei distort towards a direction which corresponds to an optimum for interatomic electronic sharing (= delocalization).

Table 4. Optimized bondlengths and total energy E of the C_{60} molecule, C_{60}^{6-} and C_{60}^{12-} according to *ab initio* calculations with a 3-21 G* basis set. The bondlengths are given in pm and the energy in a.ũ. We have used the GAMESS program.

System	6-6	6-5	Energy
C_{60}	138.82	144.20	–2259.0476
C_{60}^{6-}	141.78	144.11	–2257.5083
C_{60}^{12-}	150.50	144.47	–2251.8624

5. Resume and Microscopic Explanation of the Results

It has been one purpose of the present theoretical investigation to analyze the modification of the C_{60} (π) electronic structure in alkali- and alkaline-earth-doped fullerides as a function of the electron count on the soccerball. The solid state data have been supplemented by results evaluated for the molecular species C_{60}, C_{60}^{6-} and C_{60}^{12-}. The model calculations have reproduced the experimentally observed high abitity of the C_{60} unit to accept excess electrons without reducing the overall strength of the π bonding. With increasing metal-to-C_{60} CT a continuous transition between two π electronic boundary configurations has been observed. These are the configurations denoted as I and II in Figure 7. But note that the SCF wave function of all systems under consideration neither corresponds to the bare structure I nor to II. As a function of the electron count in the C_{60} unit both boundary configurations can be approached more or less. The SCF state of C_{60} and doped fullerides with a lower concentration of doping atoms is quite close to configuration I, while II is approached in highly doped materials. Let us mention concisely the oxidation state of the alkali and alkaline-earth donor atoms as derived in the present CO approach. Both atoms deviate strongly from the limit of complete valence ionization. Ba is more or less monovalent. The Ba-C_{60} bonding is provided by approximately the same amount of ionic and covalent interactions. Both contributions are also found in the potassium-doped fullerides. Here, this cooperative effect requires an oxidation state of potassium < 1.0. We have emphasized in detail that the K oxidation state depends on the interstitial site. The graduation we have observed can be explained by straightforward arguments. With decreasing size of the cage around the dopant atom the covalent coupling can compete successfully with the long-range Coulomb attraction between atoms with net charges of different sign. Although it is well-known that the covalence of alkali- and alkaline-earth-carbon bonds is overestimated by Hamiltonians of the present type, we are convinced that the incomplete CT derived by the present CO model is not a computational artefact but describes some electronic peculiarities of doped fullerides. In Ba_xC_{60} systems, strong hydridization has been discussed in many publications [11, 29 - 32]. But also in the case of the potassium-doped fullerides several experimental observations have been mentioned in the foregoing sections that suggest an incomplete CT [21, 35 - 37].

Starting point of our study has been the presentation of the results of electronic structure calculations. A microscopic explanation of these findings, however, has not been given up to now. This will be the endpoint of the present article. To rationalize the electronic peculiarities of the C_{60} fragment with different electron count, it is sufficient to concentrate on one pentagon defect. Let us consider this element in C_{60}^{12-}. In picture II (see Fig. 7), e. g., 12 decoupled pentagons with six π electrons per cyclic fragment occur. The basic principles of our argumentation are not influenced by the π/σ non-orthogonality of the C_{60} system. These effects are small in comparison to the phenomena discussed below. For the following discussion it is necessary to mention concisely previous theoretical findings. In recent contributions we have shown that the π electron ensemble in cyclic and branched geometries alternatively can either exhibit the quantum statistics of a fermionic (fe) or a so-called hard core bosonic (hcb) system [55 - 57]. The quantum degrees of freedom of fermionic systems are restricted by two constraints, i) the Pauli exclusion principle (PEP) not to find two electrons of the same spin direction at the same center (= same atomic orbital) and ii) the Pauli antisymmetry principle (PAP) which states that the electronic wave function changes the sign whenever the sequence of two electrons of the same spin direction is changed. Both constraints reduce the interatomic sharing (= delocalization) and lead to an energetic destabilization. In hard core bosonic ensembles, the PEP is activated only while the PAP has the character of a hidden variable. Consequently, no PAP-based destabilization can occur in systems obeying the quantum statistics of an hcb ensemble. In recent contributions [55 - 57] it has been emphasized that (hydro)carbon π systems are stable if they can maximize the hcb properties and minimize the fermionic constraints. With decreasing influence of the PAP the electronic delocalization is enhanced. According to the Heisenberg uncertainty principle this is accompanied by an energetic stabilization. The activation or deactivation of the Pauli antisymmetry principle is caused by the number of electronic interchanges per spin direction if one electron is moved over the atomic sites of the many-electron system. Only in the case of an odd number of such interchanges the PAP has an influence on electronic expectation values; see below.

It is thus evident that this quantum statistical effect depends both on the molecular topology and on the number of (π) electrons. In polyenes, e. g., one has the situation that the PEP prevents any change in the ordering of the π electrons of one spin direction. Consequently the PAP is not activated and the corresponding π ensemble shows hard core bosonic properties. We wish to emphasize that electrons are undistinguishable. Therefore different distributions of the electrons, see below, are distinguished by the occupation/non-occupation of the atomic centers only.

With these background informations we move to Fig. 9, where we have symbolized on the rhs. an isolated fragment with an electron configuration derived from picture II (upper half). Remember the restriction to a single pentagon defect, i. e. a 6π system without delocalization across the 6-6 bonds. In the lower half of the figure we have shown symbolically one possible many-electron configuration formed by three π electrons of one spin direction in a basis of atomic occupation numbers. In short, the circles in the diagram denote the occupation of the different atomic centers by π electrons of a given spin direction. The arrow indicates that one electron is transferred from center 5 to center 1 under the influence of the kinetic energy part of the Hamiltonian. Thereby the electrons localized at centers 2 and 3 have been passed by (change of the π electron ordering). In the case of the fragment configuration derived from II, two electronic interchanges take place. Quantum statistics tells us that any even number of electronic interchanges conserves the sign of the matrix elements defined by the kinetic energy part of the Hamiltonian. Here the PAP has no influence on the electronic properties of the system. Consequently the π electron transfer symbolized on the rhs. of Fig. 9 leads to an energetic stabilization. Note that also all other nearest-neighbour moves allowed by the PEP conserve the electronic ordering. We are left with the situation that the PAP is deactivated in cyclic π units with ($2n$+1) electrons per spin direction ($n = 0, 1, 2, \ldots$). In these molecules the π electron ensemble shows hcb characteristics, a behaviour which can be considered as the microscopic origin of "aromatic stabilization". Of course this ($2n$+1) π electron count per spin direction reproduces the famous Hückel ($4n$+2) rule derived for cyclic annulenes [58]. In short, the microscopic origin leading to the stabilization of ($4n$+2) annulenes lies in the deactivation of the PAP. To come back to C_{60}^{12-}; the formation of 12 island structures of 6π electron pentagon defects requires π electron moves across the 6-5 bonds (partial double bond character).

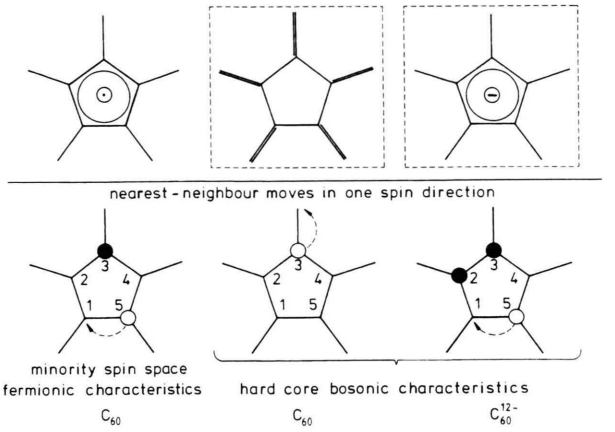

Fig. 9. Upper half: Possible electronic configurations accessible for an isolated pentagon and 5-radialene defect of C_{60} and C_{60}^{12-}. In the middle we have shown schematically the fragment electronic structure derived from picture I of Fig. 7 (6-6 double bonds) and on the rhs. the fragment electronic structure derived from picture II of Fig. 7 (6-5 bonds with partial double bond character). The latter configuration requires one excess electron per pentagon unit. On the lhs. we have symbolized the pendant of the 6-5 arrangement shown on the rhs. in neutral C_{60} leading to five π electrons per pentagon. Lower half: One possible electron configuration of the π electrons of one spin direction that is in line with the above "resonance structures". In the adopted representation of atomic occupation numbers, each circle symbolizes the occupation of a certain atom by one electron. On the lhs. we have displayed a two-electron configuration of the minority spin space of the 5π electron pentagon unit, while the configuration on the rhs. refers to the π electrons of one spin direction in the presence of one excess electron per pentagon. In the middle we have shown one π electron of a localized 6-6 double bond. The atomic numbers define the ordering of the (π) electrons. A jump process from center 5 to 1 (lhs, rhs.) is accompanied by a change of this ordering. On the rhs. two electrons at centers 2 and 3 are passed by, if the third electron changes its atomic position. Here the sign of the wave function is conserved. On the lhs. only one electron at center 3 has been passed by. Now the Pauli antisymmetry principle causes a sign change in the electronic wave function, a process leading to an energetic destabilization. As explained in the text, a fermionic quantum statistics is established in this case. The statistics fulfilled for the electronic ensemble on the rhs. is of the so-called hard core bosonic type. Hcb properties are also realized for the localized π ensembles shown schematically in the center part. We have symbolized the electron that changes its position by an open circle and the π electrons which have been passed by the transferred one by a full circle. Note that the circles used in Figs. 1, 8 and 9 symbolize different quantities (i. e. atomic centers, AO expansion coefficients in LMOs and atomic occupation numbers.

Let us next consider an isolated pentagon with five π electrons, i. e. an electron count that is realized in neutral C_{60}; see lhs. of Figure 9. In the lower half we again have symbolized one possible π electron move in the minority spin space. By analogy with the example just described, this process leads to an interchange in the electronic ordering. In general, any change in the ordering of the electrons requires a jump process between the two "terminal" centers of a cyclic unit (= centers 1 and M of an M-membered ring). In the majority spin space of the 5π electron pentagon, the hcb behaviour shown on the rhs. of the figure is reproduced. In contrast to this situation only one electron is passed by the transferred one in the minority spin space symbolized on the lhs. of the diagram. For such a transfer process the PAP is activated and would cause an energetic destabilization. To summarize, on the rhs. of the diagram (C_{60}^{12-} electronic structure) the 6π electron ensemble shows hcb properties, while fermionic properties are realized in the minority spin space on the lhs. (C_{60} electronic structure). How to avoid or attenuate these PAP-based constraints in neutral C_{60} and doped systems with not too high a charge excess? This is possible in the electronic configuration derived from picture I (center part of Fig. 9) with localized 6-6 bonds. In the C_{60} fragment shown in Fig. 9 this leads to a 5-radialene structure. By analogy with the electronically isolated pentagon sextet (rhs. of the figure) the PAP is deactivated in an electronic configuration with perfectly localized 6-6 two-center double bonds. In each of these units only one π electron per spin direction occurs. Problems caused by an interchange in the electronic ordering thus are irrelevant. Consequently the localized 6-6 π electron units behave as hcb ensembles. The prize that has to be paid for the avoidance of the PAP-based constraints is the localization of the π electrons within two-center units. In the picture of the "resonance structures" we have introduced in Fig. 7 one can deduce the following. The pentagon defects of C_{60} would act as destabilizing structural element whenever five π electrons are delocalized across the 6-5 bonds. In this case fermionic (PAP-based) constraints are activated. They can be avoided in configuration I with localized two-center bonds. Here the electronic system is hcb-like. In configuration I, however, some kind of topological electron localization occurs. In solid state science this is denoted as Anderson localization [59]. In [57] some of us have demonstrated that the constraints caused by the topological localization are less restrictive than the electron localization caused by the PAP (prerequisite: not too large cyclic units). In the presence of one excess electron, each pentagon unit acts as stabilizing element allowing cyclic delocalization according to hcb quantum statistics and thus an "aromatic behaviour". We wish to point out that empirical chemical intuition leading to the definition of quantities such as "aromatic π electron sextet, antiaromatic rings", etc. is rather appealing in the discussion of the π electronic properties of doped C_{60} fullerides.

Finally we have to mention that we only have given a short presentation of the microscopic origin of the variable π electron properties of the C_{60} fragment on the basis of two quantum statistics. The basic theory we have adopted in this context is exact; for further details we refer to [55 - 57]. Above we have restricted our discussion to two more or less isolated electronic subunits: "decoupled" localized two-center orbitals confined to the 6-6 bonds and "decoupled" pentagon orbitals with "leading" amplitudes from one ring, a pattern establishing a 6-5 double bond character. In the complete molecular network a non-negligible coupling between these local electronic fragments has to be expected, a process that leads to some intermixing of electronic configurations with 6-6 and 6-5 "delocalization" and thus some intermixing of the underlying quantum statistics (hcb and fe). In [55] it has been emphasized that fermionic constraints are attenuated with increasing system size (electron count). In short, in the C_{60} units a competition between the avoidance of the PAP and the tendency to maximize the number of centers where electronic sharing is possible, takes place. The balance between these two factors is a sensitive function of the net electron count on the C_{60} unit. We are convinced to have given a straightforward microscopic explanation of the fact that the C_{60} unit can act as some type of electronic switch.

Acknowledgements

This work has been supported by the Fonds der Chemischen Industrie and the Bundesministerium für Forschung und Technologie. We are grateful to Mrs. S. Breide for the preparation of the figures. Thank you to Dr. S. Philipp for critically reading the manuscript.

Appendix

In Table 5 we have summarized the CPU time and space demands required in the different theoretical steps

Table 5. CPU time and space demand necessary in the different computational steps. We have always given the CPU time for one calculation. In total we have considered 11 different solids and three molecular species (C_{60}, C_{60}^{6-}, C_{60}^{12-}). The solid state calculations and the unitary transformation of the canonical MOs to localized MOs in the molecules have been performed with the INDO approach described in [20, 39], while the GAMESS program has been used to optimize the geometry of the three molecules [40].

Computational step	Computer	CPU time	Space demand
CO calculations	SNI S400/40	8 h ($z = 2$), 1h ($z = 1$)	1 GByte
ab initio (geometry)	Pentium 133	40 h	5 MByte
MO localization	DECstation 5000/125	30 h	4 Mbyte

of the present study. We have used a Siemens-Nixdorff (SNI) supercomputer of the Computing Center of the TH Darmstadt as well as a Pentium 133 and a DEC-station. The overall theoretical analysis required more than 50 hours CPU time on the SNI supercomputer and more than 250 hours CPU time on the two PCs.

[1] R. C. Haddon, Acc. Chem. Res. **25**, 127 (1992).
[2] A. Raghunathan, Superconductors **6**, 1 (1993).
[3] W. E. Billups and M. A. Ciutolini (ed.), Buckminsterfullerenes, VCH, Weinheim 1993.
[4] H. Ehrenreich and F. Spaepen (ed.), Solid State Phys., Vol. **48**, Academic Press, Boston 1994.
[5] J. Rosseinsky, D. W. Murphy, R. M. Flemming, R. Tycko, A. P. Ramírez, T. Siegrist, G. Dabbagh, and S. E. Barrett, Nature**356**, 416 (1992).
[6] T. Tanigaki, I. Hirosawa, T. W. Ebbesen, J. Mizuki, Y. Shimakawa, Y. Kubo, J. S. Tsai, and S. Kuroshima, Nature**356**, 419 (1992).
[7] K. Holczer, O. Klein, S.-M. Huang, B. Kaner, K.-J. Fu, R. L. Whetten, and F. Dieterich, Science **252**, 1154 (1991).
[8] C. -C. Chen, S. P. Kelty, and C. M. Lieber, Science**253**, 886 (1991).
[9] A. R. Kortan, N. Kopylov, S. Glarum, E. M. Gyorny, A. P. Ramírez, R. M. Flemming, F. A. Thiel, and R. C. Haddon, Nature London **355**, 529 (1992).
[10] A. R. Kortan, N. Kopylov, S, Glarum, E. M. Gyorny, A. P. Ramírez, M. Flemming, O. Zhou, A. F. Thiel, P. L. Trevor, and R. C. Haddon, Nature London **360**, 566 (1992).
[11] S. C. Erwin and M. R. Pederson, Phys. Rev. B **47**, 14657 (1993).
[12] M. C. Böhm, T. Schedel-Niedrig, H. Werner, R. Schlögl, and J. Schulte, manuscript in preparation.
[13] S. C. Erwin, ref. [3], p. 217 and references cited therein.
[14] W. E. Pickett, ref. [4], p. 226 and references cited therein.
[15] G. E. Scuseria, ref. [3], p. 103 and references cited therein.
[16] P. W. Fowler, Philos. Mag. Lett. **66**, 277 (1992).
[17] J. Hutter and H. P. Lüthi, Int. J. Quantum Chem. **46**, 81 (1993).
[18] J. Kohanoff, W. Andreoni, and M. Parrinello, Chem. Phys. Lett. **198**, 472 (1992).
[19] P. W. Fowler and A. Ceulemans, J. Phys. Chem. **99**, 508 (1995).
[20] R. Ramírez and M. C. Böhm, Int. J. Quantum Chem. **34**, 47 (1988).
[21] J. Schulte and M. C. Böhm, Solid State Commun. **93**, 249 (1995).
[22] M. C. Böhm and J. Schulte, Physica C **252**, 282 (1995).
[23] M. C. Böhm and J. Schulte, Mol. Phys., **87**, 735 (1996).
[24] M. C. Böhm, T. Schedel-Niedrig, H. Werner, R. Schlögl, and J. Schulte, Solid State Commun., **98**, 463 (1996).
[25] M. C. Böhm, T. Schedel-Niedrig, H. Werner, R. Schlögl, and J. Schulte, Solid State Commun., in press.
[26] H. Werner, PhD Thesis, Universität Frankfurt, 1994.
[27] R. S. Mulliken, J. Chem. Phys. **23**, 1833, 1841 (1955).
[28] C. Lambert and P. v. R. Schleyer, Angew. Chem. **106**, 1187 (1994).

[29] Y. Chen, F. Stepniak, J. H. Weaver, P. F. Chibante, and R. E. Smalley, Phys. Rev. B **45**, 8845 (1992).
[30] Y. Chen, D. M. Poirier, M. B. Jost, C. Gu, T. R. Ohno, J. L. Martins, J. H. Weaver, L. P. F. Chibante, and R. E. Smalley, Phys. Rev. B **46**, 7961 (1992).
[31] S. Saito and A. Oshiyama, Solid State Commun. **83**, 107 (1992).
[32] S. Saito and A. Oshiyama, Phys. Rev. Lett. **71**, 121 (1993).
[33] D. L. Novikov, V. A. Gubanov, and A. J. Freeman, Physica C **191**, 399 (1992).
[34] S. H. Glarum, S. J. Duclos, and R. C. Haddon, J. Am. Chem. Soc. **114**, 1996 (1992).
[35] D. M. Poirier and J. H. Weaver, Phys. Rev. B **47**, 10959 (1993).
[36] T. Tanigaki, I. Hirosawa, J. Mitzuki, and T. W. Ebbesen, Chem. Phys. Lett. **213**, 395 (1993).
[37] P. J. Benning, D. M. Poirier, T. R. Ohno, Y. Chen, M. B. Jost, F. Stepniak, G. H. Kroll, J. H. Weaver, J. Fure, and R. E. Smalley, Phys. Rev. B **45**, 6348 (1992).
[38] K. B. Wiberg, Tetrahedron **24**, 1083 (1968).
[39] M. C. Böhm and R. Gleiter, Theor. Chim. Acta **59**, 127, 153 (1981).
[40] M. W. Schmidt, K. K. Baldridge, J. A. Boatz, S. T. Elbert, M. S. Gordon, J. H. Jensen, S. Koseki, N. Matsunaga, K. A. Nguyen, S. J. Su, T. L. Windus, M. Dupuis, and J. A. Montgomery, J. Comput. Chem. **14**, 1347 (1993).
[41] D. J. Axe, S. C. Moss, and D. A. Neumann, ref. [4], p. 149.
[42] O. Zhou and D. E. Cox, J. Phys. Chem. Solids **53**, 1373 (1992).
[43] J. H. Weaver, D. M. Poirier, ref. [4], p. 1.
[44] A. R. Kortan, N. Kopylov, R. M. Flemming, O. Zhou, F. A. Thiel, R. C. Haddon, and H. M. Raabe, Phys. Rev. B **47**, 13070 (1993).
[45] Y. Z. Li, J. C. Patrin, M. Chander, J. H. Weaver, L. P. F. Chibante, and R. E. Smalley, Phys. Rev. B **46**, 12914 (1992).
[46] M. C. Böhm, Lecture Notes in Chemistry, Vol. **45**, Springer, Heidelberg 1987.
[47] R. Ramírez and MC. Böhm, phys. stat. sol. (b) **135**, 551 (1986).
[48] R. A. Evarestov and V. P. Smirnov, phys. stat. sol. (b) **119**, 9 (1983).
[49] R. Ramírez and M. C. Böhm, Int. J. Quantum Chem. **34**, 571 (1988).
[50] C. Edmiston and K. Ruedenberg, Rev. Mod. Phys. **35**, 457 (1963).
[51] L. S. Wang, J. Conceicao, C. Lin, and R. E. Smalley, Chem. Phys. Lett. **182**, 5 (1991).
[52] Q. Xie, E. Pérez-Cordero, and L. Echegoyen, J. Am. Chem. Soc. **114**, 3978 (1992).
[53] J. Fagan, J. C. Calabrese, and B. Malone, Acc. Chem. Res. **25**, 134 (1992).
[54] W. England, L. S. Salmon, and K. Ruedenberg, Top. Curr. Chem. **23**, 31 (1971).
[55] J. Schütt and M. C. Böhm, Mol. Phys. **85**, 1217 (1995).
[56] J. Schütt, M. C. Böhm, and R. Ramírez, Chem. Phys. Lett. **248**, 379 (1996).
[57] J. Schütt and M. C. Böhm, submitted for publication.
[58] E. Hückel, Z. Physik **76**, 628 (1932).
[59] P. W. Anderson, Phys. Rev. **109**, 1402 (1958).